Electric field-assisted dissolution of bimetal-dielectric multilayer systems

Petar Pervan, Vesna Blažek Bregović, Jordi Sancho-Parramon, Vesna Janicki*
Ruđer Bošković Institute, Bijenička cesta, 10000, Zagreb, Croatia
e-mail: janicki@irb.hr

The electric field-assisted dissolution (EFAD) of Ag and Au metal island films (MIFs) in multilayer structures is investigated. The samples consist of Au and Ag MIFs separated by SiO_2 layers deposited on soda-lime glass substrates. The samples were subjected to two types of process: a) thermal annealing at 200 °C, and b) application of 500 V dc voltage at 200 °C. Spectroscopic ellipsometry and secondary ion mass spectroscopy were used to track sample changes. It is shown that thermal annealing induces ion exchange between Ag and Na ions from the glass, leading to partial dissolution of Ag MIFs and Ag being incorporated in the glass and Au MIF. EFAD process leads to the partial or complete dissolution of Ag films depending on the process duration, while Au dissolution turns out to be more difficult. The optical properties are consistent with the compositional changes and additionally suggest MIF morphology modifications. Numerical simulations of ion drift and diffusion reveal the importance of ion exchange during thermal annealing to enable an efficient MIF dissolution. Overall, the study helps to understand the EFAD of different metals in complex systems and provides insights for the application of this technique in systems containing several metals.

Keywords: metal island films, electric field assisted dissolution, multilayers, ion exchange, localized surface plasmon resonance.

1. Introduction

Metal island films (MIFs) are a current focus of interest due to their exotic optical response that combines the localized plasmon resonance of isolated particles, the presence of electromagnetic hot spots between closely located particles and the free-electron response in the case of percolated systems [1]. They are considered a promising candidate for plasmonic lithography-free metasurfaces and photonic devices as they can be easily produced by well-established thin film technology [2,3]. Furthermore, it is possible to easily combine MIFs with dielectric layers and broaden the achievable optical response by including interference effects in multilayer structures [4-7]. The incorporation of a second metal into the system enables additional degrees of freedom for tailoring the optical response because the optical properties of MIFs strongly depend on the metal dielectric function and its ability to wet the substrate where it is deposited [8].

The optical response of MIFs can be broadly modified with post-deposition treatments. Thermal annealing induces film dewetting and increases particle sphericity resulting in a narrowing and blueshift of the localized surface plasmon resonance [9,10]. Thermal annealing can also lead to the redistribution of metal by ion diffusion into the dielectric surrounding [11, 12]. Similarly, if a glass containing alkali ions is used as the substrate, metal diffusion is enhanced by the ion exchange process [13]. A process closely related to ion exchange is the electric field-assisted dissolution (EFAD), based on the application of electric field and temperature in order to drift metal ions and fully dissolve metal nanoparticles and films [14,15]. The selective application of electric field by using patterned electrodes has enabled the development of multiple techniques for the fabrication of 2D and 3D photonic structures [16-18].

A complete understanding of the interplay between ion drift and diffusion processes and sample structure is necessary to fully exploit the EFAD potential for optical properties tailoring. Recent studies have addressed the investigation of EFAD in thin film systems, including multilayer films with Ag nanoparticles [19] and metal films deposited on substrates coated with dielectric layers [20-22]. However, less attention has been paid to the simultaneous EFAD of different

metals. To the best of our knowledge, only the simultaneous dissolution of Au and Co has been addressed [23].

In this work , we investigate the EFAD process applied to metal-dielectric multilayer systems containing Ag and Au MIFs. Ag and Au are the most common plasmonic materials, with Au presenting higher chemical stability and Ag a stronger plasmonic response [24]. Au MIFS present broader and red-shifted plasmon resonance and percolate more easily than Ag MIFs [25, 26]. EFAD on single compact layers of these metals has shown that the dissolution process is more difficult in the case of Au [27]. The systems investigated here consist of Au and Ag MIFs separated by SiO_2 layers and deposited on soda-lime substrates. Samples with different MIF thicknesses are subjected to thermal annealing and to the EFAD process. It is shown that during thermal annealing a significant diffusion of Ag and alkali ions into the dielectric layers takes place, while Au remains less affected. Upon the application of the electric field, Ag and alkali ions drift into the glass matrix, with the Au layer being more difficult to dissolve and slowing down the drift of Ag and alkali. These compositional changes have an evident effect on the evolution of the optical properties, modifying the plasmon line shape for both Ag and Au. The results are supported by numerical simulations of the ion drift process.

2. Experimental

The coatings were deposited by electron beam evaporation on substrates pre-heated to 220 °C in a modified Varian chamber. Substrates were 1 mm thick Menzel microscope glass slides (72.2% SiO_2, 14.3% Na_2O, 6.4% CaO, 4.3% MgO, 1.2% K_2O, 1.2% Al_2O_3, 0.3% SO_3 and 0.08% Fe_2O_3). The layer mass thickness was controlled by quartz crystal monitoring. Five samples were deposited: 9 nm Au MIF in SiO_2 (glass/SiO_2/Au/SiO_2), 9 nm Ag MIF in SiO2 (glass/SiO_2/Au/SiO2), thinner Ag/Au sample with 24 nm Ag and 9 nm Au (glass/SiO_2/Ag/SiO_2/Au/SiO_2), thicker Ag/Au sample with 50 nm of Ag and 30 nm of Au (glass/SiO_2/Ag/SiO_2/Au/SiO_2) and thicker Au/Ag sample with 30 nm of Au and 50 nm of Ag (glass/SiO_2/Au/SiO_2/Ag/SiO_2). Metal layer thickness is given as mass thickness. For these deposition conditions, MIFs were not percolated. SiO_2 layers mass thickness in all the samples was 80 nm.

Annealing was done at 200 ºC for 90 min in air atmosphere. EFAD was carried out by applying 500 V to the sample using Cr electrodes. Before the voltage application, samples were pre-heated to 200 °C for 40 minutes. The treatment time was between 2.5 min and 15 min. After the voltage was switched off, samples were left to cool down to room temperature.

The samples' optical properties were measured after deposition, after annealing and after EFAD treatment by spectroscopic ellipsometry using a J.A. Wollam V-VASE ellipsometer. Statistical uncertainty of the determined ellipsometric angles Δ and Ψ was 0.1- 1%. Optical characterization was performed based on ellipsometry data using the W-VASE software, modelling the layers using a multiple oscillator approach as previously reported [25,26]. New parameters were introduced and kept only if the the function of merit of the data fitting, i.e. the discrepancy between simulated and experimental data normalized to the statistical uncertainty of the measurements, was significantly reduced. Function of merit of the final models showed typical values between 2 and 5. The compositional profile was obtained from secondary ion mass spectrometry (SIMS), using O^{2+} primary ions beam. The spectrometer resolution is 0.5 atomic mass units and therefore the investigated species signal can be well separated.

3. Results and discussion

3.1 Effects of thermal annealing

Figure 1 shows the composition of the distribution of annealed thicker Ag/Au and Au/Ag samples. In both samples, there is a significant redistribution of Ag and alkali ions (Na^+ and Ca^{2+}) while Au appears to remain at the position in which it was deposited. It turns out that Ag piles up in the Au layer. The quantity of material in MIF can be related to the intensity curve. The ratio of the Ag quantity in the Au layer to the Ag quantity in the Ag layer ([Ag@Au]/[Ag@Ag]) is approximately 0.26 in the Au/AgAu sample and 0.39 in the Ag/Au sample. Sodium piles up approximately the same in both MIF layers and can be found also in all SiO_2 layers. The ratio of the Na quantity in the Au layer to the Na quantity in the Ag layer ([Na@Au]/[Na@Ag]) is 0.83 in Au/Ag sample and 0.7 in Ag/Ausample. These observations suggest that the redistribution of Ag and Na is dominated by ion exchange and a preferential

tendency of Ag to diffuse into the Au layer. The nearly constant profile of Ca and its lack of correlation with the Ag concentration profile points out a simple diffusion process [28]. Au, due to its low diffusivity and large ionic charge (3+) is less prone to participate in the ion exchange process [29]. It has also been reported that Ag diffusion in Au is faster than Au diffusion in Ag [30], in accordance with the asymmetric behaviour of Ag and Au observed in the samples.

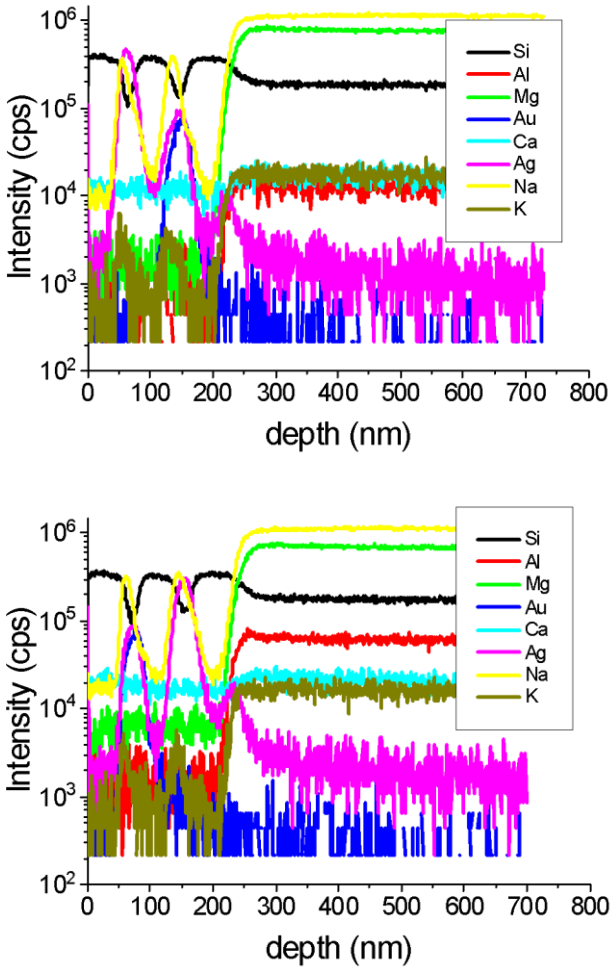

Fig 1. SIMS compositional profile of the annealed thicker Au/Ag (top) and Ag/Au (bottom) samples. The interface between the coating and glass is revealed by the steep growth of Al intensity.

Figure 2 shows the imaginary parts of the effective dielectric function of Au (top) and Ag (bottom) in as-deposited and annealed Ag MIF, Au MIF and thicker and thinner bimetal samples. In both cases, the localized surface plasmon resonance peak becomes more intense and shifts to

lower energies with the quantity of the deposited metal. This behaviour is associated with a growth of metal fraction in the MIF layer as well as an increase in the aspect ratio of particles with the amount of deposited metal, as it has been reported in several studies [25, 26, 31]. The contributions to the imaginary part of the dielectric function in Au at high photon energies (>2.5 eV) are related to the interband transitions [32]. Upon annealing, a slight shift of the plasmon resonance towards lower energies is observed in the case of Ag, which suggests a mild Ag surface oxidization [33]. There is also a small shift in the Au sample in the opposite direction. This shift is more pronounced in the case of bimetal samples A plausible explanation of this observation is that metal nanoparticles become more spherical and isolated from each other by annealing and the plasmon peak shifts towards higher energies as reported elsewhere [9, 34].

The most remarkable effect of annealing in bimetall samples is the appearance of a secondary shoulder/peak at lower photon energies than the main plasmon peak. This peak can be interpreted as a signature of interaction among the particles, that is stronger as the inter-particle distance decreases as it has been reportd in experimental studies [34, 35] and supported by numerical simulations [36]. In the case of Ag, the main peak grows and narrows with the annealing indicating the reshaping of MIF. This assumption can explain why the Ag shoulder of the thicker sample becomes more visible: although nanoparticles have become more spherical and distant, there is still a large fraction of them close enough to display this absorption feature. The thinner samples have less Ag, so the shoulders, even if present, are not so much pronounced. Au shoulder of the thinner sample grew much higher upon annealing although there is no significant change in the main peak position or shape. Such an increase in the shoulder intensity can be understood by the presence of more metal in MIF in comparison to the as-deposited sample, which can be connected with the diffusion of Ag into the Au layer revealed by SIMS. The change is less remarkable in the case of thicker layers. The mass thickness ratio of Ag to Au in the thicker samples is 5:3 and in the thinner ones 8:3, meaning that there is even less Au in comparison with Ag in the latter (thinner) one. Consequently, additional Ag seems to impact more optical properties of the thinner than the thicker MIF samples. The morphological changes in MIFs suggested by the correlation between optical and composition measurements could not be confirmed by standard characterization tecniques such as SEM or AFM due to the presence of the top SiO2 layer and will be the topic of further investigation

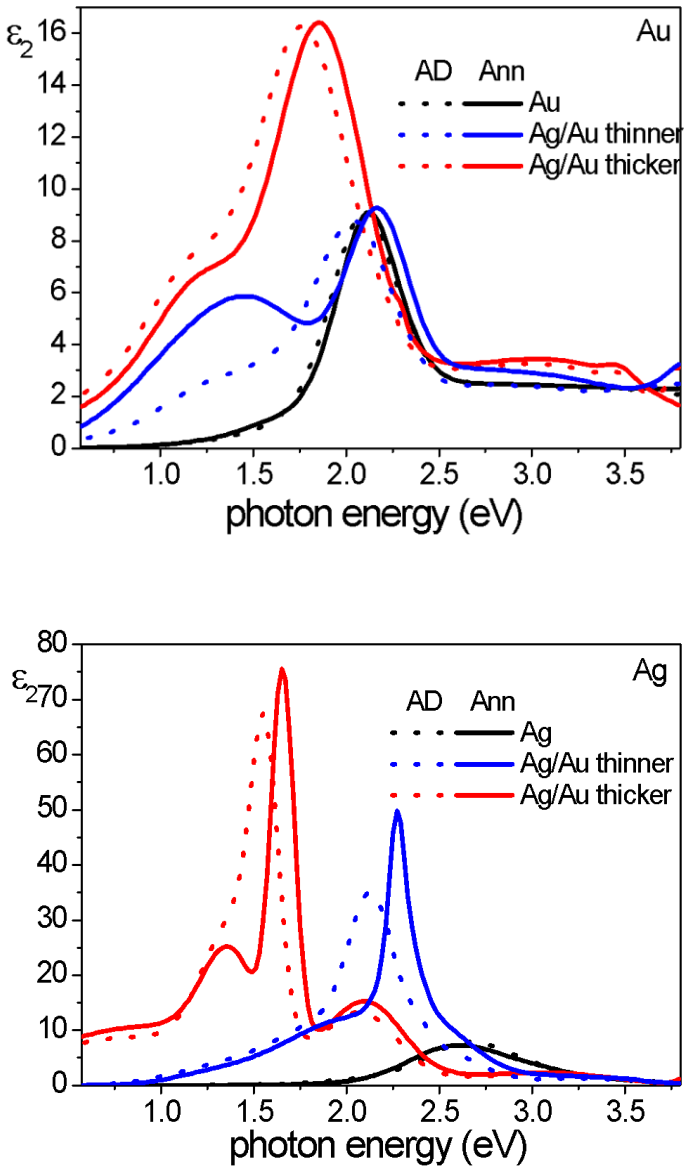

Fig.2. Imaginary part of Ag and Au effective dielectric functions for single MIFs and bimetal samples as deposited (dashed) and after annealing (solid lines). Statistical errors in effective dielectric function values, estimated from the confidence limits of parameters optimized during data fit, are up to 4%.

3.2 Electric field-assisted dissolution

Figure 3 shows the compositional profile of the thicker samples treated with 2.5 min EFAD time.

There is no clear evidence of depleted region formation in glass: most alkali ions show an abrupt change in concentration at the same position as Al. Previous SIMS studies of soda-lime-silica glass showed that under applied DC electric field alkali and alkali earth impurities move from the sample surface, while glass-former elements (Si and O) and Al remain at the same position [37]. In glasses with similar composition Al is replacing Si in glass matrix [38], i.e. it is bound in the network unlike alkali and alkali earth ions that drift upon application of electric field. Therefore, typically the position of Si intensity step is taken as a reference for glass surface. However, in this study the first layers on glass is SiO2, so characteristic step at the interface cannot be expected. Instead, Al step is taken as reference. However, a significant amount of Ag is incorporated in the glass matrix, while the distribution of Na in the MIF and SiO_2 layers is reduced. The ratio of Ag and Na quantity in the Au layer with respect to the quantity in the Ag MIF is larger than in the annealed samples ([Ag@Au]/[Ag@Ag] is 0.3 in Au/Ag sample and 0.5 in Ag/Au, while [Na@Au]/[Na@Ag] is 1.1 in Au/Ag sample and 1.6 in Ag/Au sample). This increase suggests that once incorporated in Au layer, Na and Ag ion drift is quenched. Indeed, Na and Ag tend to form alloys with Au, improving chemical stability [36, 39]. Regarding the dissolution process, this results in Ag layers losing Ag and Na faster than Au layers.

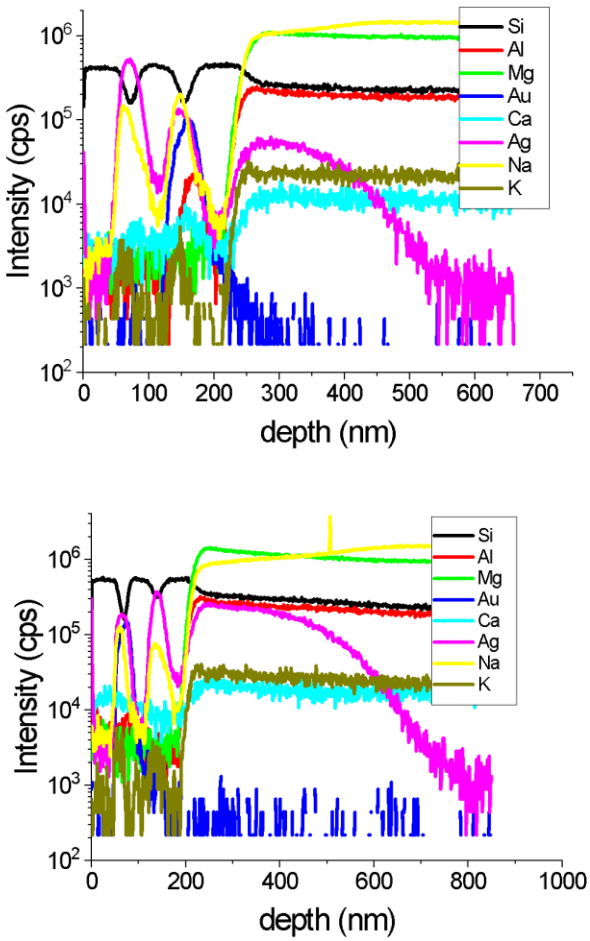

Fig 3. SIMS compositional profile of the thicker bimetall samples (top Au/Ag, bottom Ag/Au) after short EFAD treatment (2.5 min). The interface between the coating and glass is indicated by the steep growth of Al intensity.

Compositional profiles of thicker samples corresponding to longer treatment times are shown in Figure 4. In both samples, Ag has penetrated deeper into the glass compared to the short treatment times and a region with sequentially piled up Ca, Mg. This is the consequence of lower mobility of these alkalis compared to Na and Ag and the high electric field build up in Na depleted region during glass poling, a process going simultaneously with EFAD [40-43]. Pile up of Au in the sample treated for 12 min is formed as well, indicating that Au has mobility

comparable to or a bit lower than Mg. Ag penetration and depth of the pile-up region are larger for the thicker Au/Ag (EFAD time 12 min) than for the thicker Ag/Au sample (EFAD time 5 min). For both samples Na signal reduced to the noise level indicating it has returned back into glass. The Ag layer is completely dissolved, but some quantity of Ag is still present in Au layers confirming that Ag is hardly released once it diffused into Au. In both samples, a plateau of Si and Al at the glass surface is present, while the other samples have a ramp there. The plateau is wider for thicker Au/Ag sample with a longer EFAD time. It indicates densification of the glass matrix occurring due to the transition of non-bridging oxygen bonds to bridging, in lack of cations [44-46].

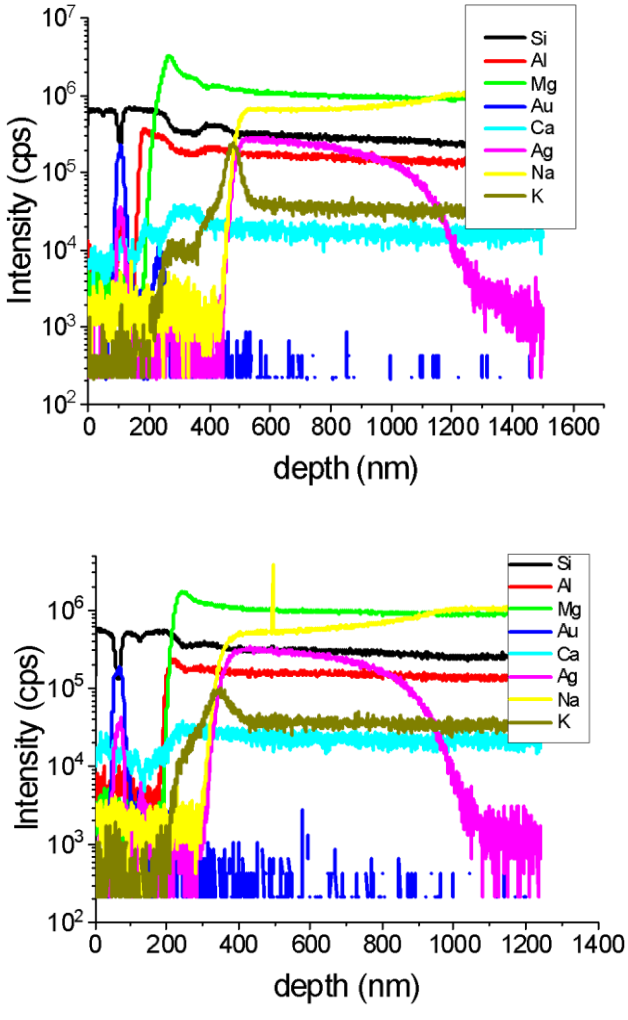

Fig 4. SIMS compositional profile of the thicker Au/Ag sample (top) and thicker Ag/Au sample (bottom)after long EFAD treatment (EFAD time 12 and 5 min, respectively). The interface between the coating and glass is indicated by the steep growth of Al intensity.

To support the evolution of the samples subjected to the EFAD treatment, numerical simulations of the ion drift and diffusion process for multiple ions [40, 47] were performed. The system of coupled differential equations describing the concentration depth-profile for each ion species is solved numerically as described in [48]. Literature values for ionic mobilities ($\mu_{Na} = \mu_{Ag} = 7x10^{-16}$ m^2V/s,$\mu_H = 2x10^{-20}$ m^2V/s) and Haven ratio (H = 0.3), initial ion concentration estimated from sample composition ($C_{Na} = 5x10^{27}$ m^{-3}, $C_{Ag} = = 1x10^{28}$ m^{-3} and voltage and temperature values applied in the experiments are used in the simulations. For the sake of simplicity, we consider Na as the only alkali species and that only Ag participates in the drift and diffusion process. Figure 5a shows the initial ion distribution assumed in the simulation, inspired by the SIMS profile of the annealed sample (Figure 1). It is assumed that Na has diffused into the SiO_2 and MIF layers and Ag has diffused into the Au layer and into the SiO_2 layer next to the interface with the glass. If blocking conditions are simulated (no injection from H^+ ions to compensate spatial charge formation upon drift of Ag and Na ions), the ion distribution displays no appreciable change from the initial composition. Under the same assumption in non-blocking conditions, the final compositional distribution after 15 minutes (Figure 5b) shows the incorporation of Ag into the glass matrix and decreased concentration in metal layers. However, the changes are small in comparison to the experimental observation. A suitable explanation is that the ionic mobility in the SiO_2 and MIF layers is larger than in glass due to the larger number of defects in thin films than in a glass matrix. Thus, if 5 times larger mobility is assumed for all ions travelling in SiO_2 and Ag layers compared to the mobility values in the glass matrix, the obtained distribution (Figure 5c) shows a much larger decrease of Ag in the MIFs and Ag incorporation into the glass matrix. Finally, it should be noted that if no ions are assumed to be present in the SiO_2 layers (neither Ag nor Na), i.e., if the composition redistribution that takes place due to thermal annealing is ignored, the simulations indicate an almost negligible incorporation of Ag into the glass matrix (Figure 5d). Hence, the ion redistribution that occurs during the pre-heating period prior to the application of the electric field is essential to induce the complete dissolution of layers within the considered duration of the EFAD treatments.

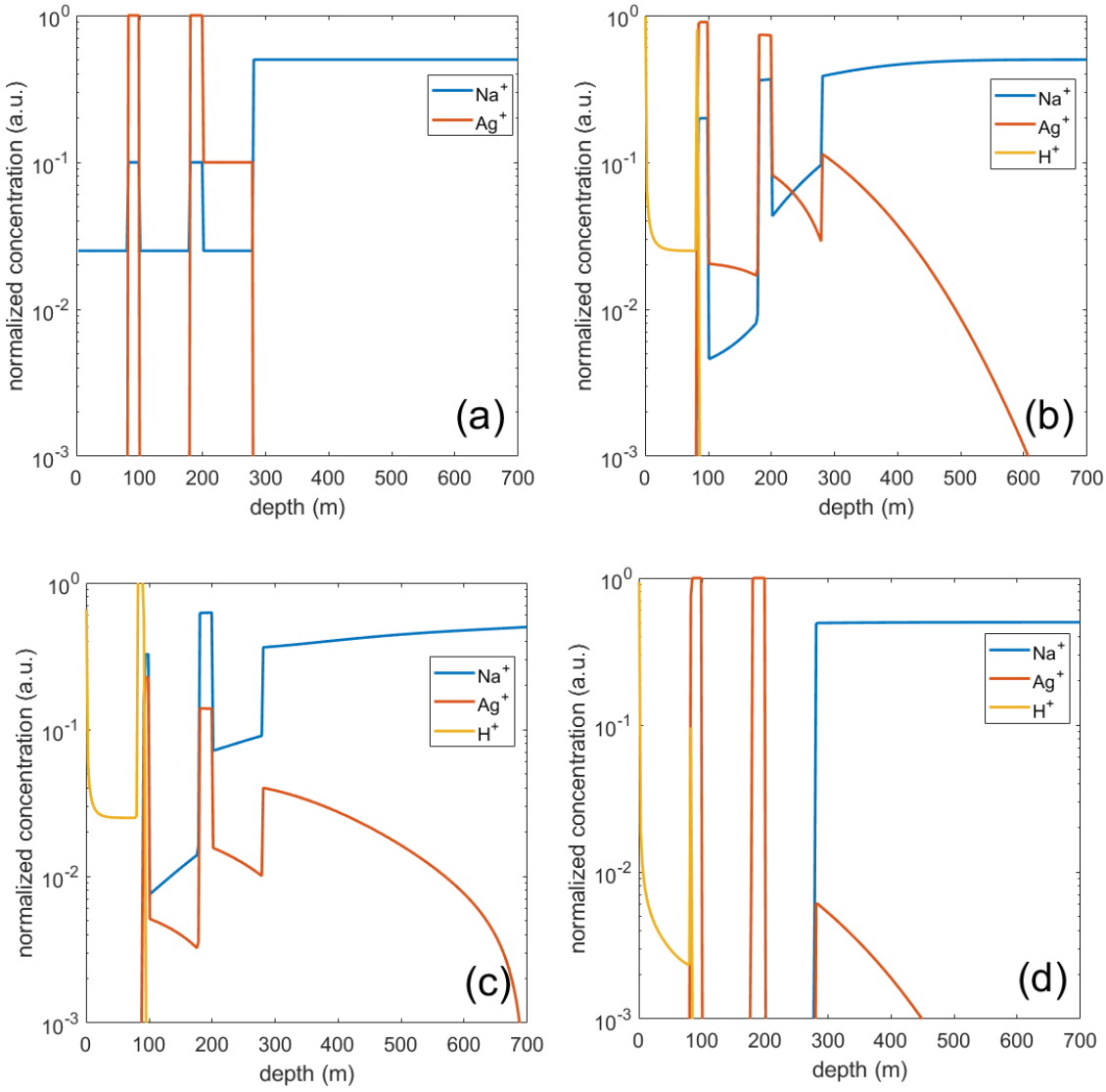

Fig 5: Numerical simulations of ion drift and diffusion process in non-blocking conditions. Initial concentration assumed for Ag and Na ions (a). Final distribution after 900 s assuming: (b) the same ionic mobility in the glass and in the multilayer structure, (c) 5 times higher ionic mobility in the multilayer structure than in glass and (d) assuming no ions are present in the SiO_2 layers.

It should be noted that the total thickness of the multilayers, as determined by the position of the Al concentration step in SIMS measurements is 30-45% smaller than obtained by optical characterization (Figure 6). This indicates a higher etching rate in the layers than in glass, especially for the samples with higher EFAD which can be expected because Ag is completely dissolved and instead Ag NPs remain pores [49, 50]. The refractive index profile also reveals a

refractive index increase in the glass regions close to the multilayer structure that can be connected to the pile-up of ionic species [48].

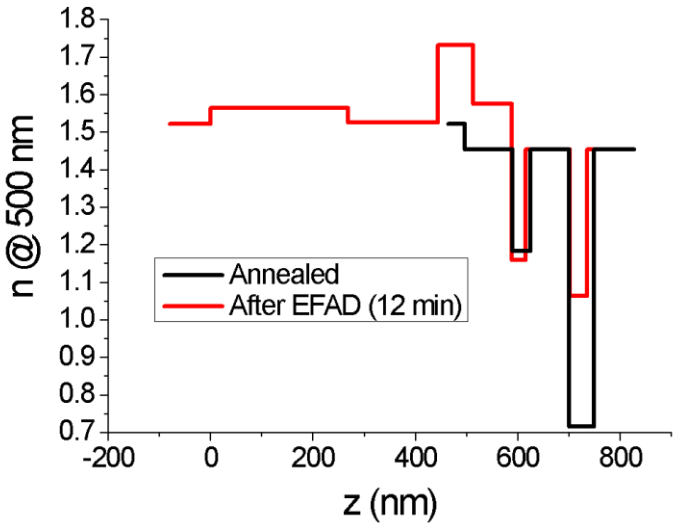

Fig 6: Refractive index profile for thicker Au/Ag sample after annealing and after EFAD with longer treatment time. Statistical errors in refractive index values, estimated from the confidence limits of parameters optimized during data fit, are up to 2%.

Indeed, when refractive index profiles are compared with SIMS measurements, it is possible to see that the increase of refractive index in glass corresponds well with the high signal of Ag that has drifted into glass (Figure 7, top). Also, in the case of the sample with the longest EFAD, refractive index peak (Fig. 7, middle and bottom) is in accordance with the position of alkali ions pile-up.

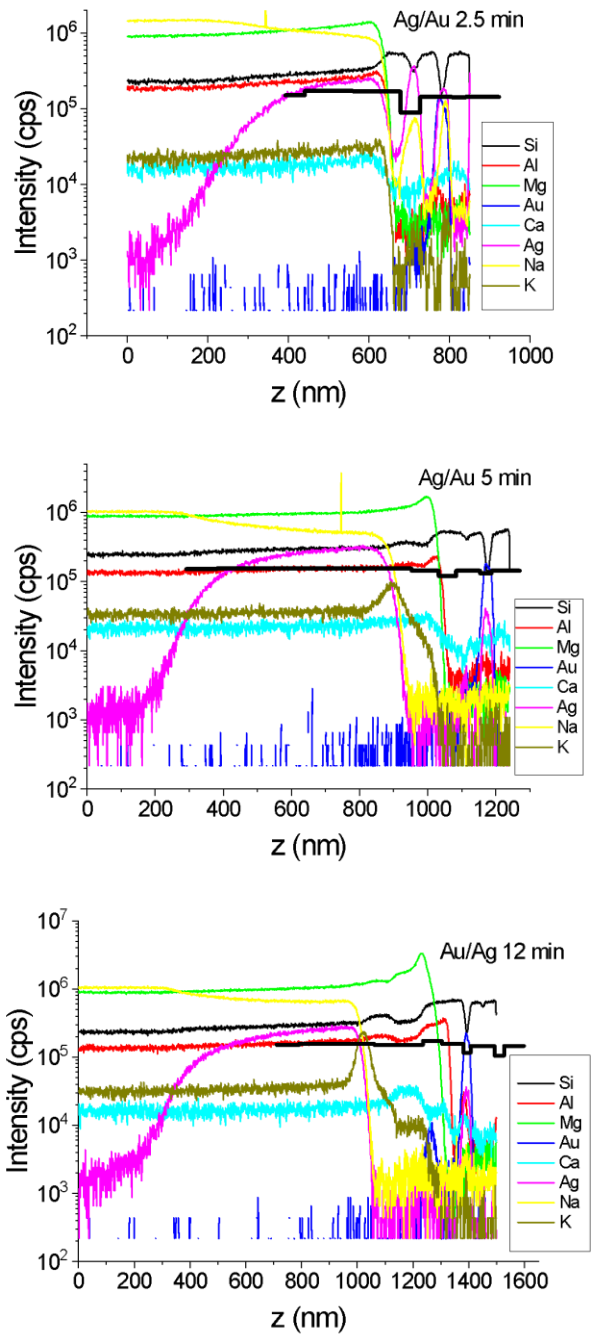

Fig 7: Comparison of SIMS measurements and refractive index profiles obtained from optical characterization. The glass/multilayers interfaces of the two have been adjusted to the same position as the reference point. This is done to compensate for the higher etching rate through the layers. Top: thicker Ag/Au sample treated for 2.5 min. Middle: thicker Ag/Au sample treated for 5 minutes. Bottom: thicker Au/Ag sample treated for 12 minutes.

Finally, we analyze the effect on the optical properties of the MIFs upon EFAD (Figure 8). A short EFAD time results in a blue shift and reduction of the localized surface plasmon resonance. This can be explained by the reduction of Ag fraction into the MIF layer upon partial dissolution of the film. Longer EFAD times lead to the complete dissolution of Ag and the total quenching of Ag-related absorption. In the case of Au MIFs, the plasmon resonance is still present even after a long annealing time, displaying only a slight red-shift and intensity decrease that is in agreement with the fact that Au remains essentially undissolved.

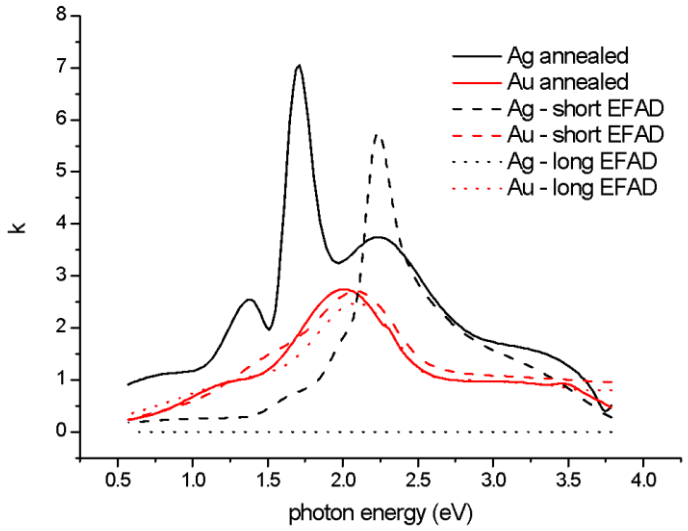

Fig 8: Extinction coefficient for the Ag and Au MIF layers of the thicker Au/Ag sample after annealing and EFAD. Statistical errors in extinction coefficient values, estimated from the confidence limits of parameters optimized during data fit, are up to 4%.

Conclusions

The influence of thermal annealing and electric field-assisted dissolution on the compositional and optical properties of multilayer structures containing Ag and Au metal island films has been investigated. Annealing of the studied bimetal systems induces optical properties changes due to MIF reshaping, but also to the interaction between metals by ion exchange. EFAD takes place

differently for Ag and Au, affecting the evolution of the sample optical properties depending on its structure.

We have determined EFAD conditions that are strong enough for the dissolution of relatively thick Ag MIF (less than 12 min) and yet too weak for considerable dissolution of Au. During annealing, Ag and Na distribute throughout the layers due to ion exchange and Ag accumulates in Au MIF. Na is found in each layer and follows Ag accumulating in Au MIF as well. While Ag and Na are removed from Ag MIF and SiO_2 layers during EFAD, some quantity of Ag remains in Au MIF. Simulations show that the ion exchange happening prior to voltage application facilitates MIF dissolution.They also show that ionic mobility should be higher in dielectric layers than in glass matrix, which is explained by defects in layers that are supporting diffusivity. Results of optical characterization are consistent with SIMS profiles, confirming it can be used for analysis of such complex systems in future research. In summary, the study provides insights that help to understand the potential application of EFAD in systems containing several metals.

References

[1] Chung T, Lee Y, Ahn MS, Lee W, Bae SI, Hwang CS, Jeong KH. Nanoislands as plasmonic materials. Nanoscale. 2019;11(18):8651-64.

[2] Ghobadi A, Hajian H, Butun B, Ozbay E. Strong light–matter interaction in lithography-free planar metamaterial perfect absorbers. ACS Photonics. 2018 Oct 30;5(11):4203-21.

[3] Liu K, Zeng X, Jiang S, Ji D, Song H, Zhang N, Gan Q. A large-scale lithography-free metasurface with spectrally tunable super absorption. Nanoscale. 2014;6(11):5599-605.

[4] V. Janicki, J. Sancho-Parramon, H. Zorc, "Gradient silver nanoparticle layers in absorbing coatings -experimental study", Appl. Opt. Vol. 50 (2011), pp. C228-C231.

[5] V. Janicki, T. V. Amotchkina, J. Sancho-Parramon, H. Zorc, M. K. Trubetskov, A. V. Tikhonravov, "Design and production of bicolour reflecting coatings with Au metal island films", Opt. Express Vol. 19(2011), pp.25521-25527.

[6] Kachan, S., Stenzel, O. and Ponyavina, A., 2006. High-absorbing gradient multilayer coatings with silver nanoparticles. *Applied Physics B*, *84*, pp.281-287.

[7] Willey, R.R. and Stenzel, O., 2023. Designing Optical Coatings with Incorporated Thin Metal Films. *Coatings*, *13*(2), p.369.

[8] Stenzel, O., 2014. Optical coatings: Material Aspects in theory and Practice.

[9] Hedl E, Bregović VB, Rakić IŠ, Mandić Š, Samec Ž, Bergmann A, Sancho-Parramon J. Optical properties of annealed nearly percolated Au thin films. Optical Materials. 2023 Jan 1;135:113237.

[10] Lee, K.C., Lin, S.J., Lin, C.H., Tsai, C.S. and Lu, Y.J., 2008. Size effect of Ag nanoparticles on surface plasmon resonance. *Surface and Coatings Technology*, *202*(22-23), pp.5339-5342.

[11] Kulczyk-Malecka, J., Kelly, P.J., West, G., Clarke, G.C.B., Ridealgh, J.A., Almtoft, K.P., Greer, A.L. and Barber, Z.H., 2014. Investigation of silver diffusion in TiO2/Ag/TiO2 coatings. *Acta materialia*, *66*, pp.396-404.

[12] Chervinskii, S., Sevriuk, V., Reduto, I. and Lipovskii, A., 2013. Formation and 2D-patterning of silver nanoisland film using thermal poling and out-diffusion from glass. *Journal of Applied Physics*, *114*(22), p.224301.

[13] Quaranta, A., Cattaruzza, E. and Gonella, F., 2008. Modelling the ion exchange process in glass: phenomenological approaches and perspectives. *Materials Science and Engineering: B*, *149*(2), pp.133-139.

[14] Podlipensky, A., Abdolvand, A., Seifert, G., Graener, H., Deparis, O. and Kazansky, P.G., 2004. Dissolution of silver nanoparticles in glass through an intense dc electric field. *The Journal of Physical Chemistry B*, *108*(46), pp.17699-17702.

[15] Lipovskii, A.A., Melehin, V.G., Petrov, M.I., Svirko, Y.P. and Zhurikhina, V.V., 2011. Bleaching versus poling: Comparison of electric field induced phenomena in glasses and glass-metal nanocomposites. *Journal of Applied Physics*, *109*(1).

[16] Janicki, V., Fabijanić, I., Okorn, B., Dubček, P. and Sancho-Parramon, J., 2018. Selective electric field assisted dissolution as a technique for micro and nano structuring of metal thin films. *Applied Physics Letters*, *113*(18), p.183508.

[17] Fabijanić, I., Okorn, B., Dubček, P., Sancho-Parramon, J. and Janicki, V., 2022. A versatile technique for micro and nano structuring of conductive thin metal layers using electric field assisted dissolution. *Materials Science in Semiconductor Processing*, *144*, p.106591.

[18] Lipovskii, A.A., Kuittinen, M., Karvinen, P., Leinonen, K., Melehin, V.G., Zhurikhina, V.V. and Svirko, Y.P., 2008. Electric field imprinting of sub-micron patterns in glass–metal nanocomposites. *Nanotechnology*, *19*(41), p.415304.

[19] Okorn, B., Sancho-Parramon, J., Pervan, P., Fabijanić, I. and Janicki, V., 2020. Evolution of electric field assisted dissolution of nanoparticles investigated by spectroscopic ellipsometry. *Optical Materials*, *101*, p.109752.

[20] Okorn, B., Sancho-Parramon, J., Oljaca, M. and Janicki, V., 2021. Metal doping of dielectric thin layers by electric field assisted film dissolution. *Journal of Non-Crystalline Solids*, *554*, p.120584.

[21] Okorn, B., Sancho-Parramon, J., Pervan, P. and Janicki, V., 2022. Electric field assisted dissolution of metal films on coated soda-lime glass. *Journal of Non-Crystalline Solids*, *591*, p.121715.

[22] Mezzapesa, F.P., Carvalho, I., Kazansky, P.G., Deparis, O., Kawazu, M. and Sakaguchi, K., 2006. Bleaching of sol-gel glass film with embedded gold nanoparticles by thermal poling. *Applied physics letters*, *89*(18).

[23] Gonella, F., Canton, P., Cattaruzza, E., Quaranta, A., Sada, C. and Vomiero, A., 2006. Field-assisted ion diffusion of transition metals for the synthesis of nanocomposite silicate glasses. *Materials Science and Engineering: C*, *26*(5-7), pp.1087-1091.

[24] West, P.R., Ishii, S., Naik, G.V., Emani, N.K., Shalaev, V.M. andBoltasseva, A., 2010. Searching for better plasmonic materials. *Laser &photonicsreviews*, *4*(6), pp.795-808.

[25] Sancho-Parramon, J., Janicki, V. and Zorc, H., 2010. On the dielectric function tuning of random metal-dielectric nanocomposites for metamaterial applications. *Optics express*, *18*(26), pp.26915-26928.

[26] Sancho-Parramon, J., Janicki, V. and Zorc, H., 2011. Tuning the effective dielectric function of thin film metal-dielectric composites by controlling the deposition temperature. *Journal of Nanophotonics*, *5*(1), pp.051805-051805.

[27] Cattaruzza, E., Gonella, F., Ali, S., Sada, C. and Quaranta, A., 2009. Silver and gold doping of SiO2 glass by solid-state field-assisted diffusion. *Journal of non-crystalline solids*, *355*(18-21), pp.1136-1139.

[28] Zhurikhina, V.V., Petrov, M.I., Sokolov, K.S. and Shustova, O.V., 2010. Ion-exchange characteristics of sodium-calcium-silicate glass: Calculation from mode spectra. *TechnicalPhysics*, *55*, pp.1447-1452.

[29] Gonella, F., Cattaruzza, E., Quaranta, A., Ali, S., Argiolas, N. and Sada, C., 2006. Diffusion behavior of transition metals in field-assisted ion-exchanged glasses. *Solid State Ionics*, *177*(35-36), pp.3151-3155.

[30] Noah, M.A., Flötotto, D., Wang, Z., Reiner, M., Hugenschmidt, C. and Mittemeijer, E.J., 2016. Interdiffusioninepitaxial, single-crystalline Au/Ag thin films studied by Auger electron spectroscopy sputter-depth profiling and positron annihilation. *Acta Materialia*, *107*, pp.133-143.

[31] Hövel, M., Gompf, B. and Dressel, M., 2010. Dielectric properties of ultrathin metal films around the percolation threshold. *Physical Review B*, *81*(3), p.035402.

[32] Palik, E.D. ed., 1998. *Handbook of optical constants of solids* (Vol. 3). Academic press.

[33] Keast, V.J., 2022. Corrosion processes of silver nanoparticles. *Applied Nanoscience*, *12*(6), pp.1859-1868.

[34] Ghosh, S.K. andPal, T., 2007. Interparticle coupling effect on the surface plasmon resonance of gold nanoparticles: from theory to applications. *Chemical reviews*, *107*(11), pp.4797-4862.

[35] de Vries, A.J., Kooij, E.S., Wormeester, H., Mewe, A.A. and Poelsema, B., 2007. Ellipsometric study of percolation in electroless deposited silver films. *Journal of applied physics*, *101*(5), p.053703.

[36] M. Bubaš, I. Fabijanić, A. Kenđel, S. Miljanić, M.C. Spadaro, J. Arbiol, V. Janicki, J. Sancho-Parramon, "Unifying stability and plasmonic properties in hybrid nanoislands: Au-Ag synergistic effects and application in SERS", Sens. Actuators B Chem., Vol. 380(2023), pp.133326.

[37] T.G. Alley, S.R.J. Brueck, M. Wiedenbeck, Secondary ion mass spectrometry study of space-charge formation in thermally poled fused silica, J.Appl.Phys. 86 (12) (1999) 6634–6640.

[38] J.E. Shelby, *Introduction to Glass Science and Technology*, The Royal Society of Chemistry, Cambridge (2005)

[39] Sarmiento-Perez, R., Cerqueira, T.F., Valencia-Jaime, I., Amsler, M., Goedecker, S., Botti, S., Marques, M.A. andRomero, A.H., 2013. Sodium–gold binaries: novel structures for ionic compounds from an ab-initio structural search. *New journal of physics*, *15*(11), p.115007.

[40] Petrov, M.I., Lepen'kin, Y.A. and Lipovskii, A.A., 2012. Polarization of glass containing fast and slow ions. *Journal of Applied Physics*, *112*(4), p.043101.

[41] A. L. R. Brennand and J. S. Wilkinson, "Planar waveguides in multicomponent glasses fabricated by field-driven differential drift of cations," Opt. Lett. 27, 906–908 (2002).

[42] R. G. Gossink, "SIMS analysis of a field-assisted glass-to-metal seal," J. Am. Ceram. Soc. 61, 539–540 (1978).

[43] I. Fabijanić, P. Pervan, B. Okorn, J. Sancho-Parramon and V. Janicki, »Ellipsometry-based study of glass refractive index depth profiles obtained by applying different poling conditions,« *Applied Optics,* vol. 59, no. 5, pp. A69-A74, 2020.

[44] M. Dussauze, V. Rodriguez, A. Lipovskii, M. Petrov, C. Smith, K. Richardson, T. Cardinal, E. Fargin and E. I. Kamitsos, »How Does Thermal Poling Affect the Structure of Soda-Lime Glass?,« *Journal of Phyical Chemistry C,* vol. 114, no. 29, pp. 12754–12759, 2010.,

[45] A. Dergachev, V. Kaasik, A. Lipovskii, V. Melehin, A. Redkov, I. Reshetov and D. Tagantsev, »Control of soda-lime glass surface crystallization with thermal poling,«*Journal of Non-Crystalline Solids,* vol. 533, p. 119899, 2020.,

[46] M. Dussauze, T. Cremoux, F. Adamietz and V. Rodriguez, »Thermal Poling of Optical Glasses: Mechanisms and Second-Order Optical Properties,«*International Journal of Applied Glass Science,* vol. 3, no. 4, pp. 309-320, 2012.).

[47] Oven, R., 2021. Analytical model of electric field assisted ion diffusion into glass containing two indigenous mobile species, with application to poling. *Journal of Non-Crystalline Solids*, *553*, p.120476.

[48] Pervan, P., Sancho-Parramon, J., Okorn, B. and Janicki, V., 2023. Modelling of concentration profiles in thermally poled glasses and correlation with refractive index profiles. *Journal of Non-Crystalline Solids*, *608*, p.122232.

[49] Zou, Z., Wang, Q., Chen, X. and Qu, S., 2009. Direct evidence for electric field assisted dissolution of Au nanoparticles on glass surface. *Journal of Applied Physics*, *105*(10).

[50] Leitner, M., Peterlik, H., Sepiol, B., Graener, H., Beleites, M. and Seifert, G., 2009. Uniformly oriented, ellipsoidal nanovoids in glass created by electric-field-assisted dissolution of metallic nanoparticles. *Physical Review B*, *79*(15), p.153408.